Research Article Vol. 31, No. 9 / 24 Apr 2023 / Optics Express 14389
Optics EXPRESS

High-fidelity ghost diffraction through complex scattering media using a modified Gerchberg-Saxton algorithm

YiNing Hao,[1] Yin Xiao,[1] and Wen Chen[1,2,*]

[1]Department of Electronic and Information Engineering, The Hong Kong Polytechnic University, Hong Kong, China
[2]Photonics Research Institute, The Hong Kong Polytechnic University, Hong Kong, China
[*]owen.chen@polyu.edu.hk

Abstract: In this paper, we propose a modified Gerchberg-Saxton (GS) algorithm to generate random amplitude-only patterns as information carriers in ghost diffraction. With the generated random patterns, high-fidelity ghost diffraction through complex scattering media can be realized with a single-pixel detector. The modified GS algorithm adopts a support constraint in the image plane, which is divided into a target region and a support region. In the Fourier plane, amplitude of the Fourier spectrum is scaled to regulate the sum of the image function. A random amplitude-only pattern can be generated to encode a pixel of the data to be transmitted using the modified GS algorithm. Optical experiments are conducted to verify the proposed method in complex scattering environments, e.g., dynamic and turbid water with non-line-of-sight (NLOS). Experimental results demonstrate that the proposed ghost diffraction is of high fidelity and high robustness against complex scattering media. It is expected that an avenue could be opened up for ghost diffraction and transmission in complex media.

1. Introduction

The concept of ghost imaging (GI) or ghost diffraction was proposed based on spatial correlation between two light beams. The first experimental demonstration of GI was performed with entangled photon pairs, and it was interpreted as quantum phenomenon [1]. Later, the successful demonstration of GI using pseudo-thermal light has brought GI to classical domain [2,3]. Since then, GI has received an extensive study, and several milestones have been achieved. Computation ghost imaging (CGI) uses a spatial light modulator (SLM) to realize light correlation with random patterns, and requires only one single-pixel detector to measure object information [4,5]. Signal-to-noise ratio (SNR) of the retrieved ghost can be improved by differential or normalization methods [6,7]. Moreover, the number of measurements in GI can be reduced by applying compressive sensing (CS) [8,9]. As GI can acquire the spatial image of an object with only a single-pixel detector, it outperforms traditional imaging techniques in non-visible wavebands [10–13] and scattering environments [14–17].

It has always been a challenge to realize high-fidelity information retrieval through complex scattering media. The difficulty is that the received data suffers from speckle noise, which is caused by the interference between distorted wavefronts [18,19]. Complex scattering media are commonly encountered in many applications, e.g., information retrieval through biological tissue and turbid water [20–22]. Over the past decade, many methods have been studied to mitigate the scattering effect, such as adaptive optics, wavefront shaping and speckle correlation [23–27]. Although adaptive optics can make corrections on the aberrations, it requires *prior* calibrations. Wavefront shaping can focus light through scattering but at the cost of a long acquisition sequence and a huge computational burden. The methods using speckle correlation are limited by memory effect, and thus are applicable to weak or thin scattering media. Moreover,

#486123 https://doi.org/10.1364/OE.486123
Journal © 2023 Received 19 Jan 2023; revised 24 Feb 2023; accepted 3 Mar 2023; published 17 Apr 2023

Optics EXPRESS

there are few demonstrations of optical analog-signal transmission through scattering media [28]. Ghost diffraction is of a great potential for analog-signal retrieval through complex scattering media. Although random patterns could be used in ghost diffraction, they have seldom been effectively designed as information carriers. Therefore, it is meaningful to explore a new method that uses random patterns as information carriers to realize high-fidelity ghost diffraction in complex scattering media.

The Gerchberg-Saxton (GS) algorithm was originally proposed to solve phase retrieval problems, which recovers unknown phase from two intensity measurements [29]. The GS algorithm alternates between the object plane and the Fourier plane. During the alternations, amplitude function in each plane is replaced by the measured intensities or a known distribution. Significant improvements have been made to deal with the stagnation problem that commonly occurs in the GS algorithm [30–32]. The hybrid input-output algorithm proposed by Fienup is especially effective in terms of increasing the convergence speed, and is widely adopted. Other modified GS algorithms are no longer confined to using Fourier transform, but rather broaden the transform domain to a larger diversity like Fresnel, fractional Fourier, and non-unitary transforms [33–35]. The development of GS algorithm opens up a wide range of applications, including optical encoding, beam shaping and holography [36–40]. The process of computer-generated hologram (CGH) generation using a modified GS algorithm iteratively encodes 3D information of the target object to a hologram. Inspired by the calculations of CGH, it is possible to modify the GS algorithm so that the pixels of the data to be transmitted can be encoded into random amplitude-only patterns. Then, the generated random patterns can be used as information carriers in ghost diffraction.

In this paper, we propose a modified GS algorithm to encode analog signals into random amplitude-only patterns, which are then employed as information carriers in ghost diffraction. The modified GS algorithm encodes pixel information in the data to a random pattern by constraining the corresponding amplitude in the Fourier plane. In the image plane, amplitude freedom is introduced. The concept of amplitude freedom refers to adding a support region around the target pattern by zero padding. Therefore, the function in the image domain contains two parts, i.e., a target region and a support region. During each iteration, the values in the support region are suppressed to zero so that the total energy would gradually cluster within the target region, which yields a better convergence. The random amplitude-only patterns generated by the modified GS algorithm are uploaded to a SLM. The SLM is illuminated by coherent light source. The modulated light then propagates through scattering media, and is finally collected by a single-pixel detector. Optical experiments are conducted in complex scattering media, and experimental results demonstrate that the proposed method is capable of realizing high-fidelity and high-robustness ghost diffraction through complex scattering media.

2. Principle

To use random patterns as information carriers [41–43], each pixel value of the data to be transmitted can be encoded into a random pattern. A modified GS algorithm is proposed to regulate the sum of a random amplitude-only pattern with a specific value. In the Fourier plane, amplitude of the Fourier spectrum is scaled to drive the sum of the pattern to approach the target pixel value. In the image plane, amplitude freedom is introduced for a fast convergence by dividing the image function into two regions. The strategy is shown in Fig. 1, where the image function consists of a target region and a support region. The target region contains a random pattern, and the support region is suppressed to zero in each iteration. The ratio between the support region and the target region can have an effect on the convergence of the modified GS algorithm. To achieve a satisfactory convergence rate, a typical ratio could be 3.

The iterative process of the proposed GS algorithm is illustrated in Fig. 2. First, a random amplitude-only pattern with 512×512 pixels is padded with zeros to have a size of 1024×1024

Optics EXPRESS

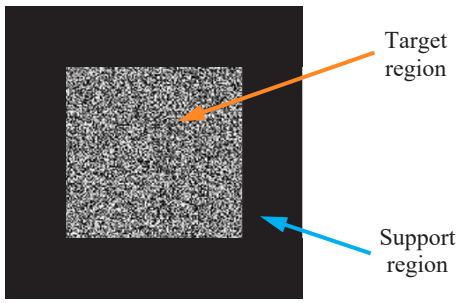

Fig. 1. A schematic illustration of the strategy to introduce amplitude freedom in the image plane of the modified GS algorithm: The image function is divided into a target region and a support region. The target region contains a random pattern, and the support region contains zeros.

pixels. The padded pattern is used as an initial input of the modified GS algorithm. During each iteration, the algorithm switches repeatedly between the image plane and Fourier plane via Fourier transform and inverse Fourier transform. The proposed algorithm can be generalized as the following four steps:

(1) Apply Fourier transform to the image g_k;

(2) Scale amplitude of the resultant spectrum G_k by a factor β;

(3) Apply an inverse Fourier transform to the updated spectrum G_k';

(4) Apply a support constraint to the resultant image g_k'.

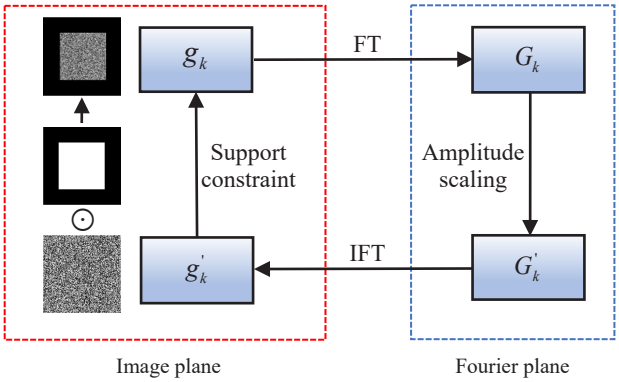

Fig. 2. A block diagram of the modified GS algorithm. FT: Fourier transform; IFT: Inverse Fourier transform.

The factor β is defined by

$$\beta = e^{(p-q)/p}, \tag{1}$$

where p denotes the target pixel value and q denotes the sum of g_k.

As can be seen in Fig. 2, the updated function g_k' contains random values in the target and support regions. A support matrix is used to suppress the values in the support region of g_k' to be zero by an element-wise multiplication. The support matrix has ones in the target region and zeros in the support region, as illustrated in Fig. 2. The input function for the next iteration is

Optics EXPRESS

also shown in Fig. 2, in which the target region contains a random pattern and the support region contains zeros. For the kth iteration, the proposed algorithm is described by

$$G_k(\xi,\eta) = \mathrm{FT}[g_k(x,y)] = |G_k(\xi,\eta)|e^{i\varphi_k(\xi,\eta)}, \tag{2}$$

$$|F(\xi,\eta)| = \beta|G_k(\xi,\eta)|, \tag{3}$$

$$G'_k(\xi,\eta) = |F(\xi,\eta)|e^{i\varphi_k(\xi,\eta)}, \tag{4}$$

$$g'_k(x,y) = \mathrm{IFT}[G'_k(\xi,\eta)], \tag{5}$$

$$g_{k+1}(x,y) = \begin{cases} g'_k(x,y) & (x,y) \notin S \\ 0 & (x,y) \in S \end{cases}, \tag{6}$$

where FT denotes Fourier transform, φ_k denotes phase distribution, IFT denotes inverse Fourier transform, and S denotes a support region. Throughout the iterative process, scaling amplitude of the Fourier spectrum can drive the sum of image function towards the target pixel value. On the other hand, the support constraint gradually forces the energy in the image plane to gather in the target region. Therefore, the proposed modified GS algorithm ultimately produces an image function that contains a random pattern whose sum is equal to the target pixel value in the target region and all zeros in the support region. Then, the target region of the output is extracted to be used as an information carrier. Pseudocode of the modified GS algorithm is given in Algorithm 1. The proposed encoding strategy can suppress scattering effect in complex environments, and realize high-fidelity signal retrieval at the receiving end as shown in the experimental results given in Section 3.

Algorithm 1: Pseudocode of a modified GS algorithm

Input: A target pixel value p to be encoded into a 2D pattern.

Initialize $g(x,y)$.
$q = \sum g(x,y)$
while $q \neq p$ **do**
  $G(\xi,\eta) = \mathrm{FT}\left[g(x,y)\right] = \left|G(\xi,\eta)\right| e^{i\varphi(\xi,\eta)}$,
  $\beta = e^{(p-q)/p}$,
  $\left|F(\xi,\eta)\right| = \beta\left|G(\xi,\eta)\right|$,
  $G'(\xi,\eta) = \left|F(\xi,\eta)\right| e^{i\varphi(\xi,\eta)}$,
  $g'(x,y) = \mathrm{IFT}\left[G'(\xi,\eta)\right]$,
  $g(x,y) \leftarrow g'(x,y)$,
  $q = \sum g(x,y)$.
end

Output: A pattern $g(x,y)$.

For each pixel of the analog signal to be transmitted, a corresponding random amplitude-only pattern is generated by the modified GS algorithm. The sum of the generated pattern is equal to a corresponding pixel value. The modified GS algorithm can be guaranteed to quickly converge, and needs ~30 iterations (i.e., ~0.5 s on average) to encode each pixel value of the signal. A flow chart for generating a series of random amplitude-only patterns is shown in Fig. 3. However, the generated patterns may contain negative values, which cannot be displayed by the SLM. In order to solve this problem, optical experiment is conducted in a differential manner by splitting each

Optics EXPRESS

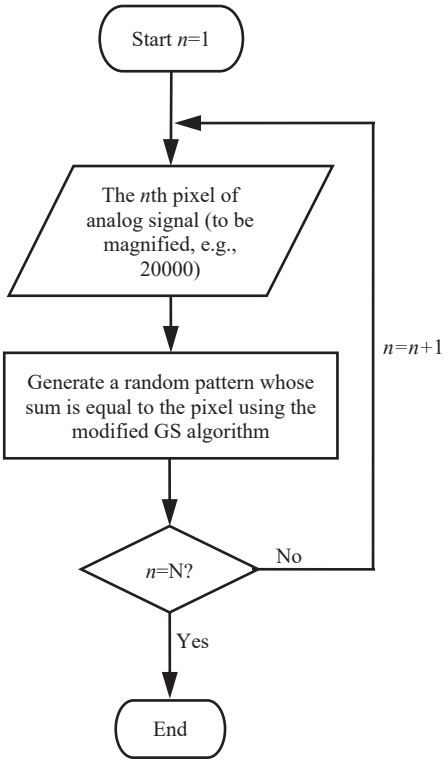

Fig. 3. A flow chart of the overall process for generating a series of random amplitude-only patterns as information carriers.

generated pattern P into two amplitude-only patterns, i.e., $m + P$ and m-P where m denotes a constant.

The generated random amplitude-only patterns are displayed by the SLM to modulate light beam. The modulated light then propagates through a dynamic and turbid water environment, which is produced with skimmed milk drops and a stirrer. At the receiving end, a single-pixel bucket detector is used to collect the scattered light. It is important to consider that scaling factor of optical system is not constant during the ghost diffraction as scattering media are highly dynamic. In this case, a direct calculation of the pixel values with a differential method cannot remove the errors caused by the varying scaling factors.

To address this issue, a fixed reference pattern P_{ref} is used before each random pattern to correct the effect brought by the scaling factors. Therefore, the recording process can be expressed by

$$B_{r1} = \lambda_1 \iint P_{\text{ref}}(x, y)\, e^{-2\pi j(x\xi+y\eta)} dxdy|_{\xi=0,\eta=0}, \tag{7}$$

$$B_1 = \lambda_1 \iint [m + P(x, y)]\, e^{-2\pi j(x\xi+y\eta)} dxdy|_{\xi=0,\eta=0}, \tag{8}$$

$$B_{r2} = \lambda_2 \iint P_{\text{ref}}(x, y) e^{-2\pi j(x\xi+y\eta)} dxdy|_{\xi=0,\eta=0}, \tag{9}$$

$$B_2 = \lambda_2 \iint [m - P(x, y)]\, e^{-2\pi j(x\xi+y\eta)} dxdy|_{\xi=0,\eta=0}, \tag{10}$$

where B_{r1} denotes the first intensity value measured with the reference pattern, B_1 denotes an intensity value measured with a pattern $m + P$, B_{r2} denotes another intensity value measured with

Optics EXPRESS

the reference pattern, B_2 denotes an intensity value measured with a pattern m-P, $j = \sqrt{-1}$, λ_1 and λ_2 denote scaling factors of optical system, and (x,y) and (ξ,η) denote the coordinates in spatial domain and frequency domain, respectively. To make it clear, scaling factor is assumed to be invariant during the recording of B_{r1} and B_1 as well as during the recording of B_{r2} and B_2. Based on this assumption, the scaling effect can be eliminated by dividing B_1 and B_2 by B_{r1} and B_{r2}, respectively. Hence, the transmitted analog signal B can be retrieved by

$$B = \frac{B_1}{B_{r1}} - \frac{B_2}{B_{r2}} = \frac{2\iint P(x,y)dxdy}{\iint P_{\text{ref}}(x,y)dxdy}. \tag{11}$$

Given that the sum of P_{ref} is known, the sum of each generated pattern P can be derived from the value B. When the sum of the generated pattern P is derived, the transmitted data can then be retrieved. In the proposed ghost diffraction, B is calculated according to Eq. (11) for each pixel of the data to be transmitted, and then the signal can be retrieved at the receiving end.

3. Experimental results and discussion

The proposed method is validated by a series of optical experiments. The detail of experimental setup is shown in Fig. 4, in which the light is emitted by a laser with a wavelength of 532 nm and then expanded by an objective lens with a magnification factor of 40. A lens with a focal length of 100 mm is used to collimate the expanded laser beam. After the collimation, the light is reflected by a mirror and illuminates an amplitude-only SLM (Holoeye, LC-R720), which sequentially displays the generated random patterns. The modulated light further propagates through scattering media, which consist of dynamic and turbid water with non-line-of-sight (NLOS). Finally, the scattered light is collected by a single-pixel bucket detector.

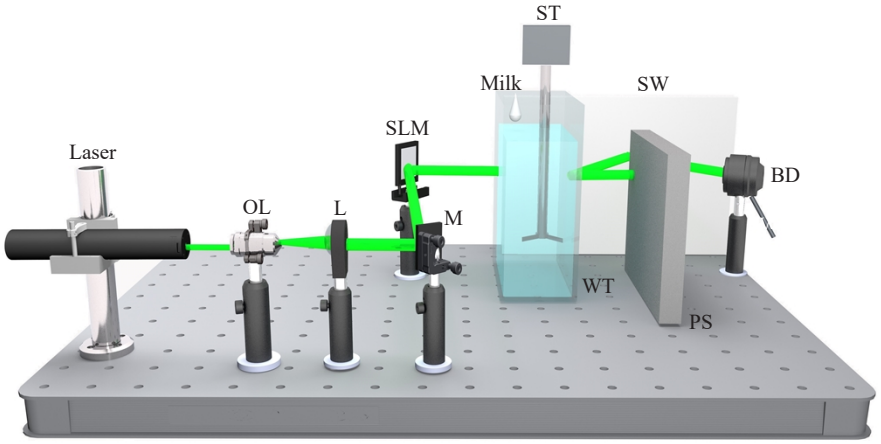

Fig. 4. A schematic experimental setup for the proposed ghost diffraction: OL, Objective lens; L, Lens; SLM, Spatial light modulator; M, Mirror; WT, Water tank; ST, Stirrer; SW, Scattering wall; PS, Protective screen; BD, Bucket detector (single pixel).

The proposed method is first tested in a dynamic and turbid water environment. As shown in Fig. 4, skimmed milk is constantly dropped into a water tank containing 3200 mL clear water. The dimensions of water tank are 100 mm (L), 150 mm (W) and 300 mm (H). A stirrer is used to evenly mix the milk drops with the water in the water tank. The propagation distance of the light in water tank is 100 mm. Three different one-dimensional (1D) analog signals are transmitted in the experiments. During each experiment, 10 mL skimmed milk is diluted with 300 mL clear water. The diluted milk is dropped constantly into water tank with a funnel, and speed of the stirrer is 1000 revolutions per minute (rpm).

Optics EXPRESS

The comparisons between original signals and the experimentally received signals are shown

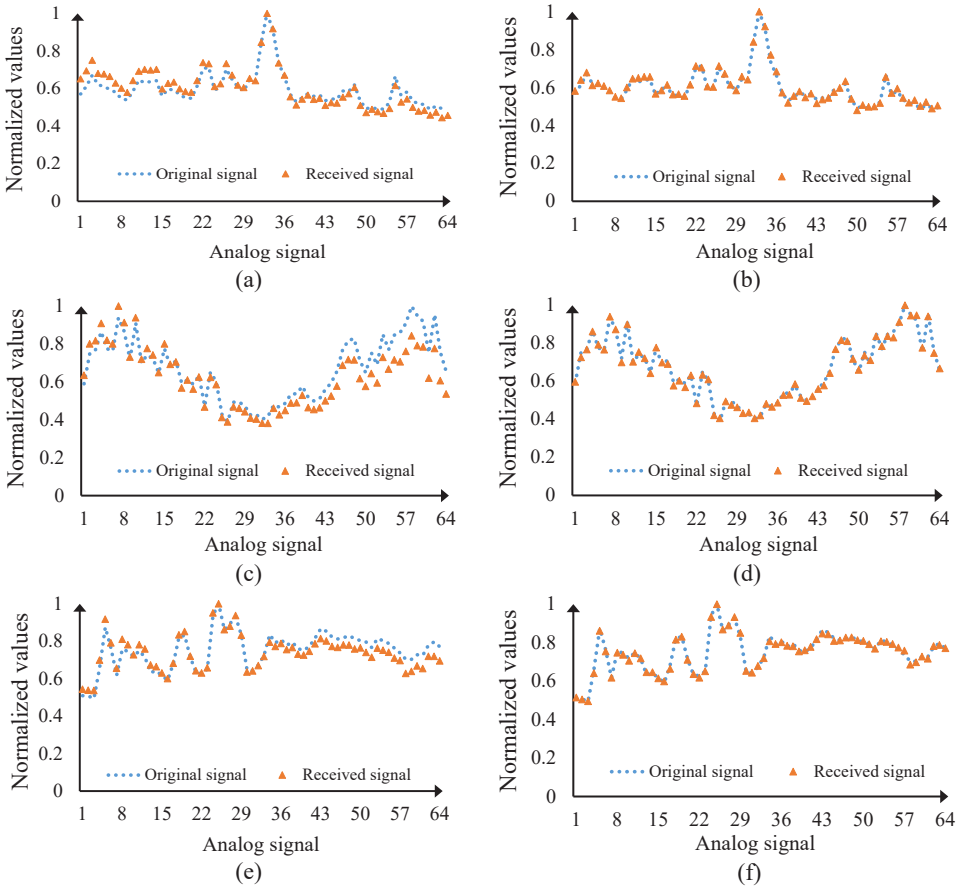

Fig. 5. Experimental results measured through dynamic and turbid water for three different signals: (a), (c) and (e) comparisons of original and received signals without using reference patterns. (b), (d) and (f) Comparisons of original and received signals using reference patterns. PSNR values of the received signals without using reference patterns in (a), (c) and (e) are 28.47 dB, 22.37 dB and 28.20 dB, respectively. MSE values of the received signals without using reference patterns in (a), (c) and (e) are 1.42×10^{-3}, 5.79×10^{-3} and 1.42×10^{-3}, respectively. PSNR values of the received signals (b), (d) and (f) using reference patterns are 38.19 dB, 38.31 dB and 40.96 dB, respectively. MSE values of the received signals using reference patterns in (b), (d) and (f) are 1.52×10^{-4}, 1.48×10^{-4} and 8.02×10^{-5}, respectively.

in Fig. 5. Specifically, the comparisons between original signals and the signals received without using reference patterns are shown in Figs. 5(a), 5(c) and 5(e). Although the original and received signals have similar shapes, there are still offsets between the original and received signals when reference patterns are not used. The offsets are caused by the variation of scaling factors in a dynamic environment, and are obvious when the concentration of skimmed milk in the water increases. In contrast, original signals and the received signals match well when reference patterns are used, as can be seen in Figs. 5(b), 5(d) and 5(f). Furthermore, peak signal-to-noise ratio (PSNR) and mean squared error (MSE) are calculated to quantitatively evaluate quality of the received signals. PSNR and MSE values of the received signals are annotated in Fig. 5. The signals received using reference patterns have high PSNR values and low MSE values, which

Optics EXPRESS

indicates that the proposed method can realize high-fidelity ghost diffraction through dynamic and turbid water.

When skimmed milk is dropped into clear water, the suspended skimmed milk particles absorb and scatter the incident light. The absorption and scattering can greatly attenuate the light intensity. It is certain that if more skimmed milk is added to the water tank, water turbidity will grow higher. Then, the attenuation effect will also be stronger. To test performance of the proposed method under different levels of attenuation, several optical experiments that use different volumes of skimmed milk are further carried out. During the experiments, the concentration of skimmed milk in the water tank is increased from 0 to 25 mL. The stirring speed remains unchanged (i.e., 1000 rpm), and wave propagation distance in scattering media is fixed (i.e., 100 mm). Beer-Lambert law describes a relationship between light intensity attenuation and characteristics of scattering media that the light propagates through. The law can be expressed by [44]

$$I(d) = I_0 e^{-\mu d}, \tag{12}$$

where $I(d)$ denotes light intensity after propagating a distance d in scattering media, I_0 denotes incident light intensity, and μ denotes the attenuation coefficient. Considering that skimmed milk is dropped into the water tank constantly, it is difficult to precisely quantify the skimmed milk concentration in water tank at a specific moment. Therefore, the change in the attenuation coefficients is used to reflect the change in water turbidity, which is due to the increase in skimmed milk concentration in water tank.

PSNR values of the received signals and the received light power under different attenuation coefficients are shown in Fig. 6(a). PSNR value of the received signal drops from 38.98 dB to 20.20 dB, and the received light power drops from 1120 nW to 73 nW as attenuation coefficient increases from 0.018 mm^{-1} to 0.036 mm^{-1}. Comparisons between original and received signals under different attenuation coefficients are shown in Figs. 6(b) and 6(c). The received signal in Fig. 6(b) is obtained, when the attenuation coefficient is 0.018 mm^{-1}. The received signal in Fig. 6(c) is obtained, when the attenuation coefficient is 0.034 mm^{-1}. As can be seen in Fig. 6(b), the received signal overlaps with original signal when the attenuation coefficient is small. However, the error in the received signal appears to be prominent as shown in Fig. 6(c) when the attenuation coefficient becomes relatively large. Hence, the proposed method can realize high-fidelity ghost diffraction when attenuation coefficient of scattering media is smaller than 0.034 mm^{-1}.

In addition to the concentration of skimmed milk, the stirring speed is also an important factor that can affect the change of attenuation coefficients. To comprehensively evaluate robustness of the proposed method, effect of the stirring speed on quality of the received signals is also investigated. In the same manner, the propagation distance of the light in scattering media is fixed at 100 mm, and the volume of added skimmed milk is fixed at 10 mL. In this case, stirring speed is the only factor that changes during the experiment. Six different stirring speeds (i.e., 1000 rpm, 1200 rpm, 1400 rpm, 1600 rpm, 1800rpm and 2000rpm) are tested in the experiments. PSNR values of the received signal and the received signal power under different stirring speeds are shown in Fig. 7. PSNR value of the received signal drops from 41.06 dB to 28.32 dB. The received light power drops from 1500 nW to 500 nW as the stirring speed increases from 1000 rpm to 2000rpm. When the stirring speed is less than 1800rpm, the received signals are of high quality and PSNR values of the received signals are above 38 dB. The high PSNR values prove that the proposed method is robust against high stirring speeds. However, it is worth noting that there is a sudden drop in the PSNR values when the stirring speed reaches 2000rpm. This is mainly caused by the increased number of turbulences and bubbles in the water that may block the light path. The results in Figs. 5–7 demonstrate that the proposed method can realize high-fidelity and high-robustness ghost diffraction in dynamic and turbid water environments.

Optics EXPRESS

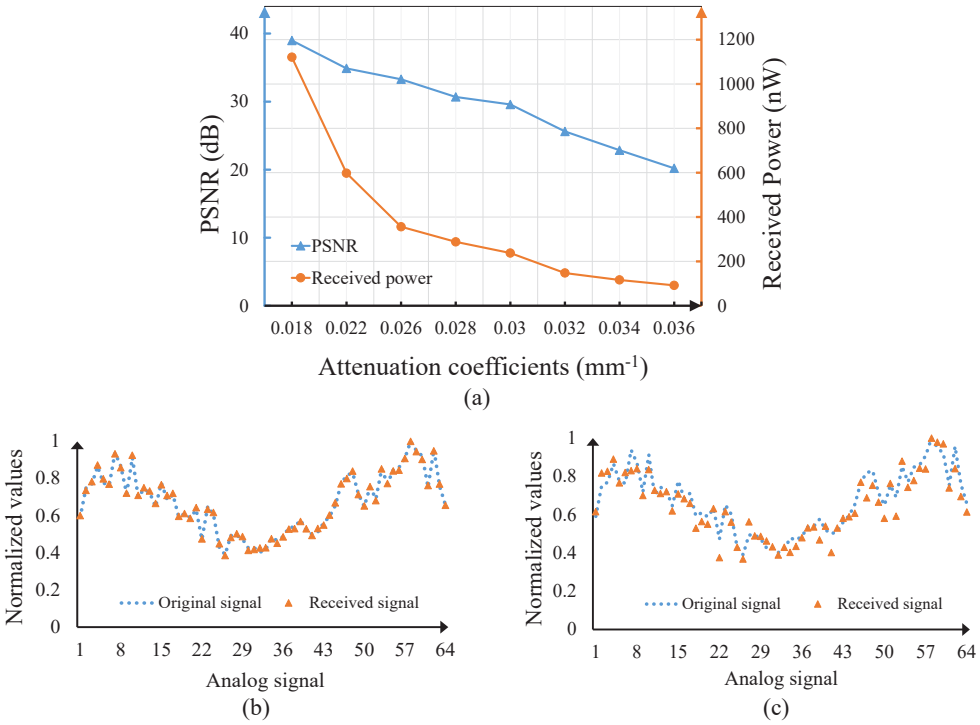

Fig. 6. (a) PSNR values of the received signals and the received light power as attenuation coefficient increases, (b) a comparison between original and received signals when attenuation coefficient is 0.018 mm^{-1}, and (c) a comparison between original and received signals when attenuation coefficient is 0.034 mm^{-1}.

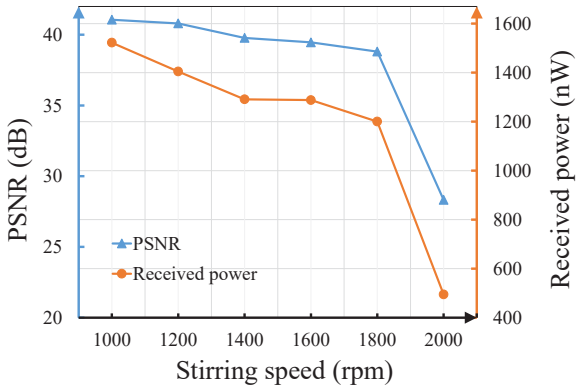

Fig. 7. PSNR values of the received signals and the received light power with different stirring speeds (rpm).

To verify capability of the proposed method, a corner is further placed between water tank and single-pixel bucket detector to partially block the light. In this case, the proposed method is tested in dynamic and turbid water with NLOS. As can be seen in Fig. 4, the corner consists of a protective screen that completely blocks the light and a scattering wall that reflects the light. After the light is scattered by dynamic and turbid water, part of the light is blocked by the protective screen and the others are reflected by scattering wall. At the receiving end, the

Optics EXPRESS

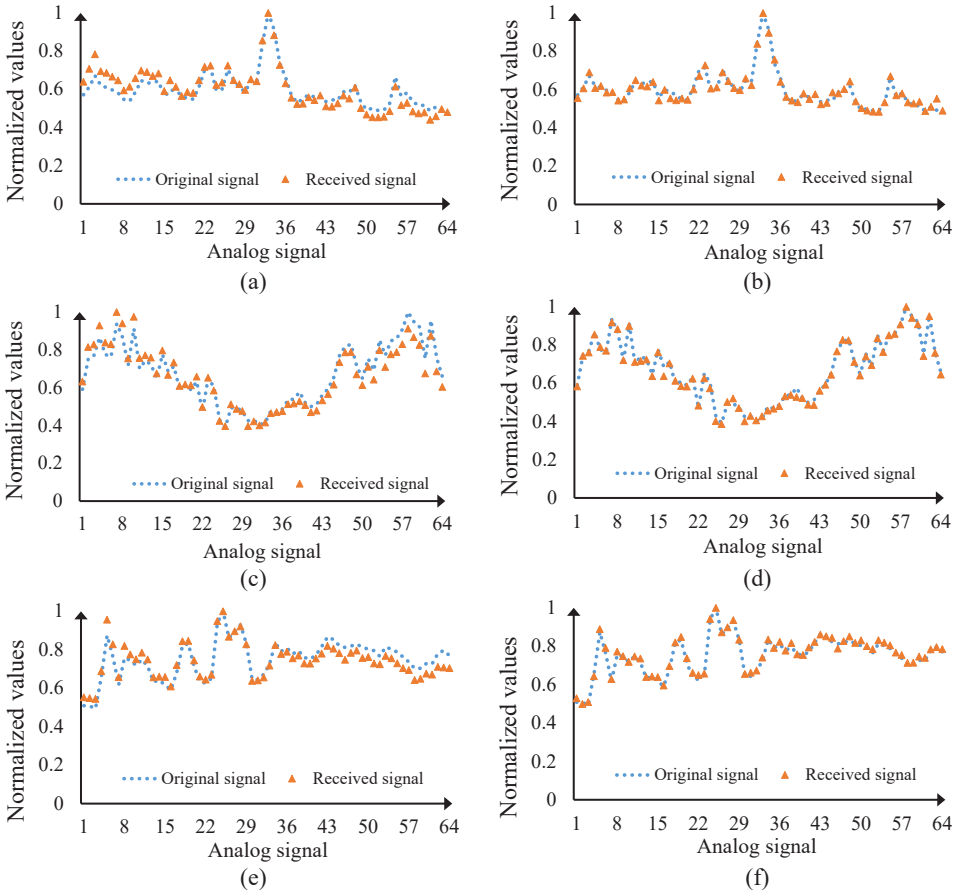

Fig. 8. Experimental results obtained in a dynamic and turbid water environment with a corner for three different signals: (a), (c) and (e) comparisons of original and received signals without using reference patterns. (b), (d) and (f) Comparisons of original and received signals using reference patterns. PSNR values of the received signals without using reference patterns in (a), (c) and (e) are 27.52 dB, 26.75 dB and 27.76 dB, respectively. MSE values of the received signals without using reference patterns in (a), (c) and (e) are 1.76×10^{-3}, 2.11×10^{-3} and 1.67×10^{-3}, respectively. PSNR values of the received signals (b), (d) and (f) using reference patterns are 35.95 dB, 36.37 dB and 36.88 dB, respectively. MSE values of the received signals using reference patterns in (b), (d) and (f) are 2.54×10^{-4}, 2.31×10^{-4} and 2.05×10^{-4}, respectively.

light reflected by the corner is captured by a single-pixel bucket detector. The wave propagation distance in water tank is fixed at 100 mm, and speed of the stirrer is fixed at 1000 rpm. Similarly, 10 mL skimmed milk is diluted with 300 mL clear water to be dropped constantly into water tank during the experiments. The separation distance around the corner, i.e., between scattering wall and protective screen, is 20 mm.

Comparisons between original and received signals are shown in Fig. 8. Original signals and the received signals without using reference patterns are compared in Figs. 8(a), 8(c) and 8(e), in which the errors can be easily observed. When reference patterns are used, the received signals are in good concurrence with original signals as can be seen in Figs. 8(b), 8(d) and 8(f). The signals in Figs. 8(b), 8(d) and 8(f) have high PSNR values and low MSE values, which quantitatively confirms high fidelity of the received signals. Hence, the proposed method can still

Optics EXPRESS

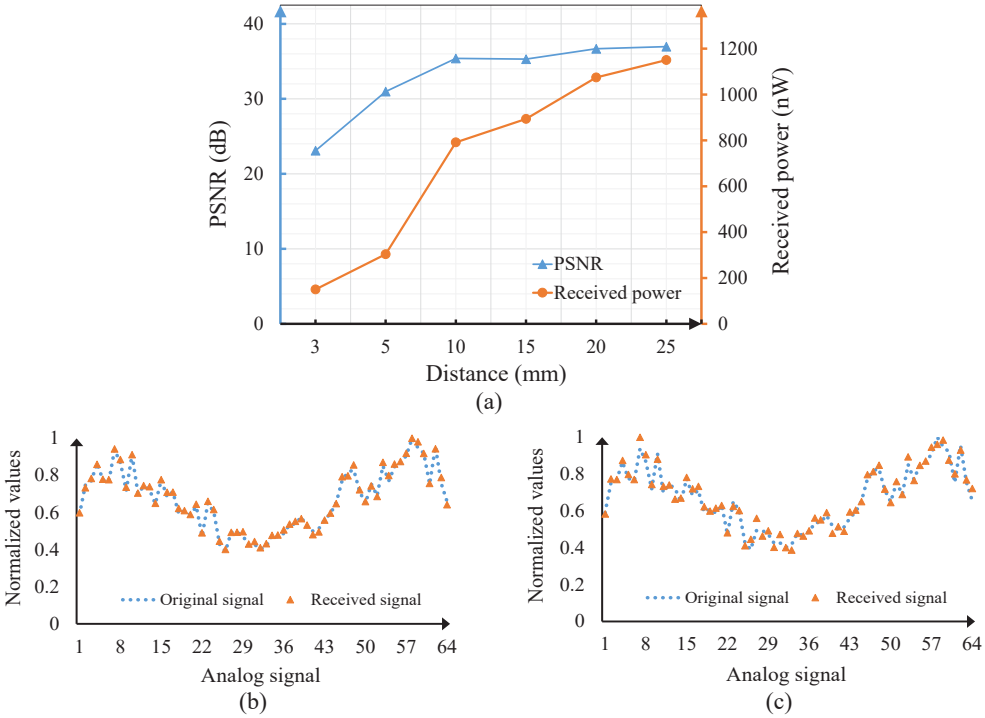

Fig. 9. (a) PSNR values of the received signals and the received light power as the separation distance around the corner varies, (b) a comparison between original and received signals when the separation distance is 25 mm, and (c) a comparison between original and received signals when the separation distance is 5 mm.

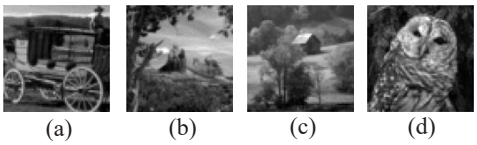

Fig. 10. (a)-(d) The experimentally retrieved images (64×64 pixels) at the receiving end.

realize high-fidelity ghost diffraction even if a corner is placed after dynamic and turbid water environment.

When the wave propagates around the corner, attenuation of light intensity is largely affected by the separation distance. Therefore, the impact of different separation distances is further studied. In the experiments, separation distance around the corner is tested with six different values, i.e., 3 mm, 5 mm, 10 mm, 15 mm, 20 mm and 25 mm. Other conditions remain the same.

PSNR values of the received signals and the received light power with different separation distances are shown in Fig. 9(a). As can be seen in Fig. 9(a), light intensity captured by single-pixel bucket detector drops dramatically from 1150 nW to 150 nW when the separation distance around the corner decreases. PSNR values of the received signals also decrease from 36.96 dB to 23.08 dB as the separation distance drops from 25 mm to 3 mm. The signals obtained at the receiving end are compared with original signal, and the results are shown in Figs. 9(b) and 9(c). The signal in Fig. 9(b) is obtained, when the separation distance around the corner is 25 mm. PSNR of the signal is 36.96 dB. Thus, the received signal is of high accuracy when the

Optics EXPRESS

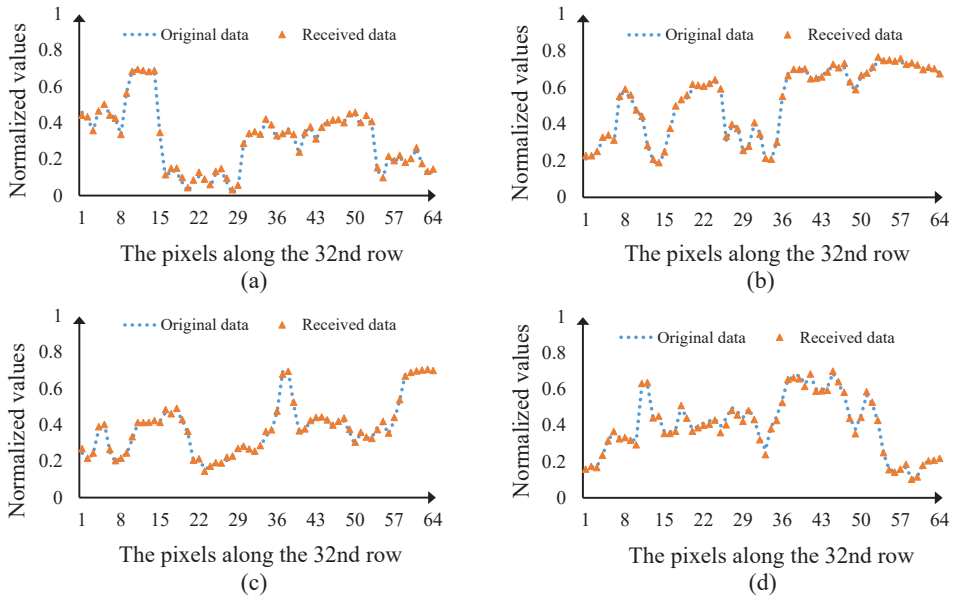

Fig. 11. (a)-(d) Comparisons between the pixels along the 32nd row of original images and those along the 32nd row of the experimentally received images in Figs. 10(a)–10(d), respectively.

separation distance is large. Moreover, the signal in Fig. 9(c) is obtained when the separation distance around the corner is 5 mm, which has a PSNR of 30.98 dB. With such a small separation distance, the received signal still matches original signal as can be seen in Fig. 9(c). When the separation distance around the corner is further reduced to 3 mm, PSNR of the received signal is 23.08 dB as most of the light is blocked by the protective screen. Hence, it is demonstrated that a high-fidelity NLOS ghost diffraction can be realized when the separation distance around the corner is not less than 5 mm.

It has been verified that analog signals can be retrieved successfully with the proposed method in dynamic and turbid water with NLOS. To further study performance of the proposed method, 2D grayscale images are encoded and tested. In this case, 2D image transmission can be realized by the proposed ghost diffraction through complex scattering media. The ghost diffraction that uses random patterns encoded with 2D grayscale images is investigated in dynamic and turbid water environment with NLOS. The conditions for dynamic and turbid water environment are the same as those in previous experiments. A corner with a separation distance of 20 mm is placed between water tank and single-pixel bucket detector as shown in Fig. 4. The experimentally received images are shown in Figs. 10(a)–10(d). PSNR and structural similarity index measure (SSIM) are utilized to quantitatively evaluate the received 2D grayscale images. PSNR values of the received images in Figs. 10(a)–10(d) are 35.96 dB, 36.19 dB, 36.16 dB and 36.60 dB, respectively. SSIM values of the received images are 0.9893, 0.9866, 0.9862 and 0.9923, respectively. Moreover, it is feasible that high-fidelity images with the larger size can also be retrieved using the proposed method.

For clarity, the pixels along the 32nd row of the received images in Figs. 10(a)–10(d) are compared with those along the 32nd row of their corresponding original images. As can be seen in Figs. 11(a)–11(d), the received data overlaps with original data. The experimental results indicate that the received images are of high fidelity. Therefore, high-fidelity 2D grayscale images can be obtained in the proposed ghost diffraction through complex scattering media.

Optics EXPRESS

4. Conclusion

In this paper, a modified GS algorithm has been proposed to encode analog signals into random amplitude-only patterns, which are used as information carriers in ghost diffraction. The modified GS algorithm regulates the sum of a random pattern by scaling the amplitude of its spectrum in the Fourier plane. In the image plane, a support constraint is used to ensure the convergence. The random patterns are generated in such a way that the sum of each pattern is equal to a specific pixel value of the data to be transmitted. In the proposed ghost diffraction, the generated random patterns sequentially modulate the light, and the encoded data can be derived from the measured intensities. Optical experiments have demonstrated that high-fidelity and high-robustness ghost diffraction can be realized in dynamic and turbid water environments with NLOS. Irregular analog signals and 2D grayscale images can be retrieved with high fidelity using the proposed method. The proposed ghost diffraction can also be realized in other scattering media, e.g., biological tissues and dynamic smoke etc. The proposed method effectively utilizes random patterns as information carriers generated by a modified GS algorithm, and successfully overcomes the challenges in analog-ghost diffraction and transmission. This work could be inspiring for the development of high-fidelity ghost diffraction and transmission in complex media, and may open up a wide range of applications in free-space optical transmission.

Funding. Basic and Applied Basic Research Foundation of Guangdong Province (2022A1515011858); Hong Kong Research Grants Council (C5011-19G, 15224921, 15223522); Hong Kong Polytechnic University (G-R006, 4-R006, 1-W167, 1-W19E, 1-BD4Q).

Disclosures. The authors declare no conflicts of interest.

Data availability. Data underlying the results presented in this paper are not publicly available at this time but may be obtained from the authors upon reasonable request.

References

1. T. B. Pittman, Y. H. Shih, D. V. Strekalov, and A. V. Sergienko, "Optical imaging by means of two-photon quantum entanglement," Phys. Rev. A **52**(5), R3429–R3432 (1995).
2. R. S. Bennink, S. J. Bentley, and R. W. Boyd, "'Two-photon' coincidence imaging with a classical source," Phys. Rev. Lett. **89**(11), 113601 (2002).
3. A. Gatti, E. Brambilla, M. Bache, and L. A. Lugiato, "Ghost imaging with thermal light: comparing entanglement and classical correlation," Phys. Rev. Lett. **93**(9), 093602 (2004).
4. J. H. Shapiro, "Computational ghost imaging," Phys. Rev. A **78**(6), 061802 (2008).
5. B. Sun, M. P. Edgar, R. Bowman, L. E. Vittert, S. Welsh, A. Bowman, and M. J. Padgett, "3D Computational imaging with single-pixel detectors," Science **340**(6134), 844–847 (2013).
6. F. Ferri, D. Magatti, L. Lugiato, and A. Gatti, "Differential ghost imaging," Phys. Rev. Lett. **104**(25), 253603 (2010).
7. B. Sun, S. S. Welsh, M. P. Edgar, J. H. Shapiro, and M. J. Padgett, "Normalized ghost imaging," Opt. Express **20**(15), 16892–16901 (2012).
8. O. Katz, Y. Bromberg, and Y. Silberberg, "Compressive ghost imaging," Appl. Phys. Lett. **95**(13), 131110 (2009).
9. P. Zerom, K. W. C. Chan, J. C. Howell, and R. W. Boyd, "Entangled-photon compressive ghost imaging," Phys. Rev. A **84**(6), 061804 (2011).
10. D. Pelliccia, A. Rack, M. Scheel, V. Cantelli, and D. M. Paganin, "Experimental x-ray ghost imaging," Phys. Rev. Lett. **117**(11), 113902 (2016).
11. W. L. Chan, K. Charan, D. Takhar, K. F. Kelly, R. G. Baraniuk, and D. M. Mittleman, "A single-pixel terahertz imaging system based on compressed sensing," Appl. Phys. Lett. **93**(12), 121105 (2008).
12. N. D. Hardy and J. H. Shapiro, "Computational ghost imaging versus imaging laser radar for three-dimensional imaging," Phys. Rev. A **87**(2), 023820 (2013).
13. G. Musarra, A. Lyons, E. Conca, Y. Altmann, F. Villa, F. Zappa, M. J. Padgett, and D. Faccio, "Non-line-of-sight three-dimensional imaging with a single-pixel camera," Phys. Rev. Appl. **12**(1), 011002 (2019).
14. P. Zhang, W. Gong, S. Xia, and S. Han, "Correlated imaging through atmospheric turbulence," Phys. Rev. A **82**(3), 033817 (2010).
15. R. E. Meyers, K. S. Deacon, and Y. Shih, "Turbulence-free ghost imaging," Appl. Phys. Lett. **98**(11), 111115 (2011).
16. P. B. Dixon, G. A. Howland, K. W. C. Chan, C. O'Sullivan-Hale, B. Rodenburg, N. D. Hardy, J. H. Shapiro, D. S. Simon, A. V. Sergienko, R. W. Boyd, and J. C. Howell, "Quantum ghost imaging through turbulence," Phys. Rev. A **83**(5), 051803 (2011).
17. M. Bina, D. Magatti, M. Molteni, A. Gatti, L. A. Lugiato, and F. Ferri, "Backscattering differential ghost imaging in turbid media," Phys. Rev. Lett. **110**(8), 083901 (2013).

Optics EXPRESS

18. J. Bertolotti, E. G. van Putten, C. Blum, A. Lagendijk, W. L. Vos, and A. P. Mosk, "Non-invasive imaging through opaque scattering layers," Nature **491**(7423), 232–234 (2012).
19. E. Tajahuerce, V. Durán, P. Clemente, E. Irles, F. Soldevila, P. Andrés, and J. Lancis, "Image transmission through dynamic scattering media by single-pixel photodetection," Opt. Express **22**(14), 16945–16955 (2014).
20. Y. M. Wang, B. Judkewitz, C. A. Dimarzio, and C. Yang, "Deep-tissue focal fluorescence imaging with digitally time-reversed ultrasound-encoded light," Nat. Commun. **3**(1), 928 (2012).
21. H. B. de Aguiar, S. Gigan, and S. Brasselet, "Enhanced nonlinear imaging through scattering media using transmission-matrix-based wave-front shaping," Phys. Rev. A **94**(4), 043830 (2016).
22. H. Lu, Y. Li, L. Zhang, and S. Serikawa, "Contrast enhancement for images in turbid water," J. Opt. Soc. Am. A **32**(5), 886–893 (2015).
23. R. Tyson, *Principles of Adaptive Optics* (Elsevier Science, Saint Louis, 1991).
24. D. Débarre, E. J. Botcherby, T. Watanabe, S. Srinivas, M. J. Booth, and T. Wilson, "Image-based adaptive optics for two-photon microscopy," Opt. Lett. **34**(16), 2495–2497 (2009).
25. J. Aulbach, B. Gjonaj, P. M. Johnson, A. P. Mosk, and A. Lagendijk, "Control of light transmission through opaque scattering media in space and time," Phys. Rev. Lett. **106**(10), 103901 (2011).
26. P. del Hougne, K. B. Yeo, P. Besnier, and M. Davy, "Coherent wave control in complex media with arbitrary wavefronts," Phys. Rev. Lett. **126**(19), 193903 (2021).
27. O. Katz, P. Heidmann, M. Fink, and S. Gigan, "Non-invasive single-shot imaging through scattering layers and around corners via speckle correlations," Nat. Photonics **8**(10), 784–790 (2014).
28. M. A. Khalighi and M. Uysal, "Survey on free space optical communication: a communication theory perspective," IEEE Commun. Surv. Tutorials **16**(4), 2231–2258 (2014).
29. R. W. Gerchberg and W. O. Saxton, "A practical algorithm for the determination of the phase from image and diffraction plane pictures," Optik **35**(2), 237 (1972).
30. D. L. Misell, "A method for the solution of the phase problem in electron microscopy," J. Phys. D: Appl. Phys. **6**(1), 102L6–L9 (1973).
31. J. R. Fienup, "Phase retrieval algorithms: a comparison," Appl. Opt. **21**(15), 2758–2769 (1982).
32. J. R. Fienup and C. C. Wackerman, "Phase-retrieval stagnation problems and solutions," J. Opt. Soc. Am. A **3**(11), 1897 (1986).
33. S. K. Rajput and N. K. Nishchal, "Fresnel domain nonlinear image encryption scheme based on Gerchberg-Saxton phase retrieval algorithm," Appl. Opt. **53**(3), 418–425 (2014).
34. Z. Zalevsky, R. G. Dorsch, and D. Mendlovic, "Gerchberg–Saxton algorithm applied in the fractional Fourier or the Fresnel domain," Opt. Lett. **21**(12), 842–844 (1996).
35. G. Z. Yang, B. Z. Dong, B. Y. Gu, J. Y. Zhuang, and O. K. Ersoy, "Gerchberg-Saxton and Yang-Gu algorithms for phase retrieval in a nonunitary transform system: a comparison," Appl. Opt. **33**(2), 209–218 (1994).
36. W. Chen, "Optical cryptosystem based on single-pixel encoding using the modified Gerchberg-Saxton algorithm with a cascaded structure," J. Opt. Soc. Am. A **33**(12), 2305–2311 (2016).
37. Z. Wang, J. Liu, X. Ding, W. Zhao, K. Zhang, H. Li, B. Ratni, S. N. Burokur, and Q. Wu, "Three-dimensional microwave holography based on broadband huygens' metasurface," Phys. Rev. Applied **13**(1), 014033 (2020).
38. L. Chen, H. Zhang, Z. He, X. Wang, L. Cao, and G. Jin, "Weighted constraint iterative algorithm for phase hologram generation," Appl. Sci. **10**(10), 3652 (2020).
39. H. Akahori, "Spectrum leveling by an iterative algorithm with a dummy area for synthesizing the kinoform," Appl. Opt. **25**(5), 802–811 (1986).
40. C. Chang, J. Xia, L. Yang, W. Lei, Z. Yang, and J. Chen, "Speckle-suppressed phase-only holographic three-dimensional display based on double-constraint Gerchberg-Saxton algorithm," Appl. Opt. **54**(23), 6994–7001 (2015).
41. Y. Xiao, L. Zhou, and W. Chen, "Wavefront control through multi-layer scattering media using single-pixel detector for high-PSNR optical transmission," Opt. Lasers Eng. **139**, 106453 (2021).
42. Y. Xiao, L. Zhou, Z. Pan, Y. Cao, and W. Chen, "Physically-secured high-fidelity free-space optical data transmission through scattering media using dynamic scaling factors," Opt. Express **30**(5), 8186–8198 (2022).
43. Y. Cao, Y. Xiao, Z. Pan, L. Zhou, and W. Chen, "Physically-secured ghost diffraction and transmission," IEEE Photon. Technol. Lett. **34**(22), 1238–1241 (2022).
44. L. Wind and W. W. Szymanski, "Quantification of scattering corrections to the Beer-Lambert law for transmittance measurements in turbid media," Meas. Sci. Technol. **13**(3), 270–275 (2002).